2014 IEEE International Conference on Robotics & Automation (ICRA)
Hong Kong Convention and Exhibition Center
May 31 - June 7, 2014. Hong Kong, China

The Development of an Innovative Two-DOF Cylindrical Drive: Design, Analysis and Preliminary Tests

Takashi Harada[1], Thomas Friedlaender[2] and Jorge Angeles[2]

Abstract— **The quest for ever faster pick-and-place robots has led to ingenious parallel robots with reduced mobility, e.g., capable of producing motions proper of SCARA systems: three independent translations and one rotation about an axis of fixed direction. These robots are also known as Schönflies-motion generators (SMG). Some parallel versions are commercially available, as are serial-parallel designs. The former are provided with four limbs, the latter with three, the fourth degree of freedom being appended in series with a Delta robot. Parallel robots are more attractive than their hybrid counterparts, but the presence of four legs poses serious challenges to their designers, as limb-interference limits the rotatability of the moving plate. A solution to this problem includes a gear train for rotation-range amplification, but this increases the inertial load on the motors and complicates the design—too many parts—and the control—because of inherent gear backlash and Coulomb friction. Recently, a SMG system was proposed that is supplied with two limbs, arrayed in an isostatic structure, which provides high rotatability of its gripper. This robot is driven by one C (cylindrical)-joint at each limb. As this joint allows for two degrees of freedom, it calls for two motors, that might as well be fixed to the base, which poses interesting design challenges. Reported in this paper is a design solution for the drive of a C joint, which is termed the C (cylindrical)-drive, based on a cylindrical differential mechanism of the RHHR type, with R standing for revolute, H for helical (or screw) joint. The design, kinematics and dynamics of the drive are discussed, along with a realization, and preliminary tests.**

I. INTRODUCTION

The motivation behind the work reported here is the need for ever faster pick-and-place robots, as required by assembly and packaging operations. The unprecedented growth in the number and variety of hand-held electronic devices calls for extremely fast robots required for the assembly of these devices, whose parts exhibit an essentially flat geometry. Another area calling for fast pick-and-place operations (PPO) is the food-processing industry, especially with regard to packaging.

The manipulation of the payload in the above application areas includes, as a rule, three independent translations and one rotation about an axis of fixed orientation, usually vertical. This kind of motion, therefore, is short of two degrees of freedom (dof)—with respect to the free motion of rigid objects in space—namely, tilt about two non-parallel, horizontal axes. The motions of interest are known to involve the set of four-dof rigid-body displacements termed the *Schönflies subgroup* [1] of the group of six-dof rigid-body motions. This subgroup can best be visualized as the set of displacements undergone by the tray of a waiter. Any mechanical system capable of producing such motions is hence termed a *Schönflies-motion generator* (SMG). The oldest SMGs date back to the early eighties, which were dubbed SCARA (Selective Compliance Assembly Robot Arm) [2]. These systems bear a serial architecture that comprises three revolute (R) joints of parallel axes and one prismatic (P) joint of direction parallel to these axes.

The industry has proposed a test cycle that consists of: a) a vertical upward translation of 25 mm; b) a horizontal 300-mm translation with a concurrent 180° rotation; c) a vertical downward 25-mm translation; and d) back to the departing pose—position and orientation—following the same path and the same motion program backwards [3]. In the late nineties, Adept Technology Inc., of Livermore, CA, boasted cycle times of their SCARA COBRA s600 of 500 ms. The same company now offers a parallel version of the old SCARA systems, the Quattro$^{\mathrm{TM}}$ s650H robot[1], reportedly capable of cycle times of 333 ms. This robot owes its origins to a concept invented by a Franco-Japanese team [4]. Further reducing the foregoing record cycle-time is the new challenge.

A hybrid SMG, ABB IRB 340 FlexPicker[2], features a Delta architecture [5], carrying three limbs that drive a moving platform (MP) through purely translational motions in 3D space. In series with the Delta system is a R joint mounted on the Delta MP, providing a rotation about a vertical axis. The latter is driven from the robot base via a Cardan, telescopic shaft. This array allows the FlexPicker to produce large-amplitude rotations. The complexity of this robot lies both in the mechanical transmission required to drive the R joint and in the *diversity* of its actuators, as the actuator of the latter is different from the three of the Delta.

A novel architecture was recently proposed that provides a high rotatability of the MP without the need of an extra transmission, and may be driven with four identical actuators [6]. Shown in Fig. 1(a) is a depiction of the proposed architecture, composed of two identical arms of the CRRH type, with the actuated C joint of each limb mounted on a fixed base. The arrows indicate the independent translation and rotation of the actuated C joints. Here, what plays the

[1]Takashi Harada is with Department of Mechanical Engineering, Faculty of Science and Engineering, Kinki University, Higashiosaka, Osaka, Japan harada@mech.kindai.ac.jp

[2]Thomas Friedlaender and Jorge Angeles are with the Department of Mechanical Engineering and the Centre for Intelligent Machines, McGill University, Montreal, QC, Canada thomasfr@cim.mcgill.ca, angeles@cim.mcgill.ca

[1]http://www.adept.com/products/robots/parallel/quattro-s650h/general

[2]http://gizmodo.com/371917/abb-flexpicker-robots-legs-move-so-fast-its-scary

role of the MP is what we call the *Peppermill*, because it is driven in a form similar to that of a waiter when spreading pepper on a diner's plate. The Peppermill is thus driven by two H-joints of distinct pitches.

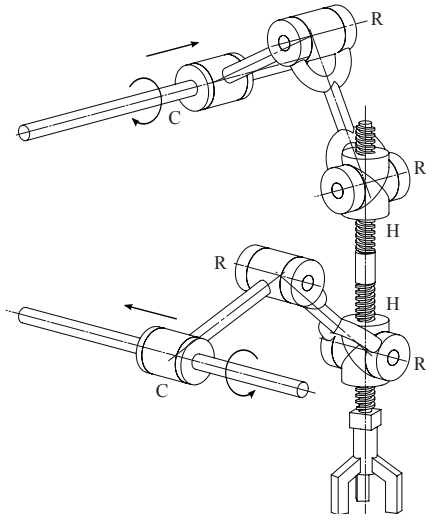

(a) The Isostatic Schönflies-motion generator [6]

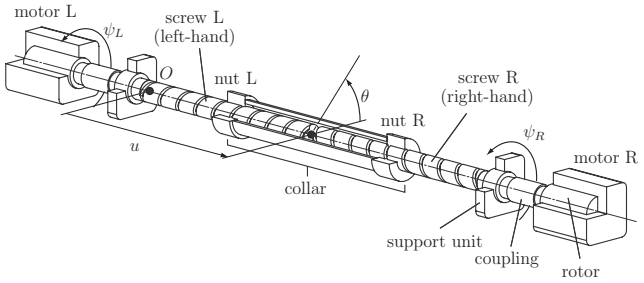

(b) The various components and variables of the C-drive

Fig. 1. The ISMG and C-drive

An interesting feature of the SMG of Fig. 1(a) is its isostatic nature, as explained in Section II. For this reason, this robot is henceforth termed the *Isostatic SMG* (ISMG).

II. DESIGN PRINCIPLES

The drives of the ISMG must implement the two dof of each limb by producing rotations and translations. This poses an interesting design challenge, as off-the-shelf actuated C joints are not available. In producing a conceptual design of the drive, the basic principle adopted is *simplicity*. To this end, the authors resort to a paradigm for the conceptual design of kinematic chains made of lower kinematic pairs (LKP)—revolute R, prismatic P, helical or screw H, cylindrical C, planar F and spherical S—based on complexity measures [7]. Moreover, the first three LKP are *simple*, in that they allow for one single dof between the links under coupling. C allows for two dof, while the last two for three.

According to the above-mentioned paradigm, the complexity of a kinematic chain grows with the number of kinematic pairs (joints), while the LKP are ordered in increasing order of complexity: R, P, H, C, F, S. Moreover, the concepts put forth by Hervé [8] on the use of Lie groups in the qualitative synthesis of kinematic chains are exploited.

Under the principle of complexity-reduction,

1) The number of joints must be as low as possible;
2) A R joint is preferred over a P joint, and a P joint over a H joint;
3) Use as many identical joints as possible, as complexity grows with their diversity.

Now, upon application of the theory of Lie groups to the synthesis of kinematic chains, a C joint can be synthesized by means of a serial array of two simple LKP: PR (or RP); RH (or HR); PH (or HP); and HH. In these arrays, the direction of motion allowed by the P joint should be parallel to the axis of the R or the H joint, while, in the case of the RH array, the two joints must be co-axial. Finally, in the case of the HH array, the two H pairs must be co-axial and of *different pitches*.

Under the ranking of the LKP by order of complexity, the simplest choice is a PR array, the most complex a HH array. However, synthesizing a C joint by means of a PR array calls for two completely different actuators, one translational and one rotational, which contributes to the actuator complexity. We thus adopt two more design principles:

4) Reduce the diversity of the actuators; and
5) for purposes of a uniform load-distribution, fix the two actuators to the base.

The first of the two foregoing principles leads to a RH array, the second to a closed kinematic chain, namely a RHHR chain, which allows for two identical rotary actuators fixed to the base. The RHHR chain can be found to have a dof $f = 2$, if the theory of Lie groups is invoked, together with the Chebyshev-Grübler-Kutzbach (CGK) formula in the version suggested by Hervé [8]:

$$f = d(l - 1) - rj \tag{1}$$

where d is the dimension of the subgroup—of the *rigid-body displacement group*—to which the chain belongs; j is the number of joints; l the number of links; and r the number of constraints imposed by the joints, under the assumption that all joints allow for the same mobility, which is the case at hand. Indeed, in our case, the chain belongs to the *cylindrical subgroup*, of dimension 2, one rotation about an axis and one translation in the direction of this axis. The number of joints is 4, while the number of links is also 4 and $r = 1$, as each joint takes away one dof of the two of the cylindrical subgroup. Therefore, $f = 2$, as desired. However, for the above formula to be correct, the pitches of the H joints must be distinct [8].

The RHHR chain is *topologically symmetric*. It can be rendered *geometrically symmetric* as well, and hence, of lowest complexity, if the two pitches are chosen identical, but of opposite hands, one right-, the other left-hand. The realization of the RHHR joint thus leads to a *cylindrical differential mechanism*, as will be made apparent in the sequel. An embodiment of the RHHR chain is included in Fig. 2.

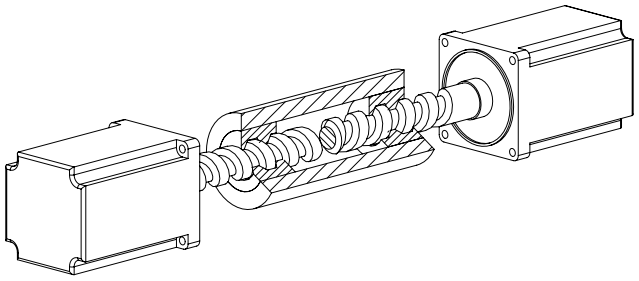

Fig. 2. An embodiment of the RHHR kinematic chain of the C-drive

Returning to the complete ISMG, upon application of the CGK formula to the kinematic chain shown in Fig. 1(a), we observe that the formula of eq. (1) applies to a chain with all its joints of the same mobility. In the chain at hand, however, the C joint has a double mobility—it allows for two dof—and hence, the above formula cannot be applied directly. For this reason, the C joint is *conceptually* decomposed into two simple joints, R and P, for example. Under these conditions, $d = 6$, $l = 10$, $j = 10$ and $r = 5$. Hence, the CGK formula yields

$$f = 6(10 - 1) - 5 \times 10 = 4 \tag{2}$$

which is the dof of a SMG. What the CGK formula does not provide is the kind of motion that this chain generates. This was done by resorting to the theory of Lie groups by the proponents of the architecture of the ISMG [6].

III. THE MATHEMATICAL MODEL

The model that describes the relations among the various parameters and the motion variables of the C joint, in both the Cartesian and the joint domains, is derived here. The kinematics of the full ISMG was derived in [9].

A. Kinematics

Figure 1(b) illustrates the design model of the driven C joint, termed C (cylindrical)-drive, as actuated by two identical rotational motors in a differential array of helical—screw—drives.

The relationships between the translational and angular displacements of the C-drive collar, u and θ, respectively, and the angular displacements of the motors, ψ_L and ψ_R, are derived below. It is apparent from Fig. 1(b) that the sliding u of the collar is proportional to either $\psi_L - \theta$ or $\psi_R - \theta$, the proportionality constant being $p_L/2\pi$ or, correspondingly, $p_R/2\pi$. Hence,

$$\frac{p_L}{2\pi}(\psi_L - \theta) = u, \quad \frac{p_R}{2\pi}(\psi_R - \theta) = u \tag{3}$$

where p_L and p_R represent the pitches of the left-hand screw and its right-hand counterpart, respectively. Moreover, notice that for the two equations (3) to be independent, and hence, useful to control the collar motion, p_L should be different from p_R. This relation is in agreement with the condition invoked from the theory of Lie groups—see Section II. In order to *simplify* the design of both the mechanical system and the control scheme of the C-drive, we introduce *symmetry* as the sixth design principle:

$$p_L = p, \quad p_R = -p \tag{4}$$

From eqs. (3 & 4), the relationships between the displacements of the collar, u and θ, and the angular displacements of the motors, ψ_L and ψ_R, are expressed by a system of two linear equations, namely,

$$\frac{p}{2\pi}\begin{bmatrix} 1 & 0 \\ 0 & -1 \end{bmatrix}\begin{bmatrix} \psi_L \\ \psi_R \end{bmatrix} = \begin{bmatrix} 1 & p/2\pi \\ 1 & -p/2\pi \end{bmatrix}\begin{bmatrix} u \\ \theta \end{bmatrix} \tag{5}$$

The inverse displacement relations, which yield the motor variables in terms of the collar variables, are

$$\begin{bmatrix} \psi_L \\ \psi_R \end{bmatrix} = \begin{bmatrix} 2\pi/p & 1 \\ -2\pi/p & 1 \end{bmatrix}\begin{bmatrix} u \\ \theta \end{bmatrix} \tag{6}$$

Likewise, the forward displacement relations are

$$\begin{bmatrix} u \\ \theta \end{bmatrix} = \begin{bmatrix} p/4\pi & -p/4\pi \\ 1/2 & 1/2 \end{bmatrix}\begin{bmatrix} \psi_L \\ \psi_R \end{bmatrix} \tag{7}$$

In order to render the actuator Jacbian $\mathbf{J}$ dimensionally homogeneous, a change of variable is introduced:

$$v \equiv \frac{p}{2\pi}\theta \tag{8}$$

Hence, relation (7) is now rewritten as

$$\mathbf{w} = \mathbf{J}\boldsymbol{\psi} \tag{9}$$

with the definitions

$$\mathbf{w} \equiv \begin{bmatrix} u \\ v \end{bmatrix}, \quad \mathbf{J} \equiv \frac{p}{4\pi}\begin{bmatrix} 1 & -1 \\ 1 & 1 \end{bmatrix}, \quad \boldsymbol{\psi} \equiv \begin{bmatrix} \psi_L \\ \psi_R \end{bmatrix} \tag{10}$$

Given the form of $\mathbf{J}$, when the two actuators turn by the same amount in the same direction, a pure rotation of the collar is produced; when the actuators turn the same amount, but in opposite directions, a pure translation is produced. This is the functioning of a *differential mechanism*.

It is noteworthy that the new form of $\mathbf{J}$ is *isotropic*, in the sense that $\mathbf{J}^T\mathbf{J}$ is proportional to the 2×2 identity matrix $\mathbf{1}$, namely,

$$\mathbf{J}^T\mathbf{J} = \frac{p^2}{8\pi^2}\mathbf{1} \tag{11}$$

Isotropy is important, because this means that the transformation from actuator variables $\boldsymbol{\psi}$ to drive variables $\mathbf{w}$, and vice-versa, is done without roundoff-error amplification [10]. Moreover,

$$\mathbf{J}^{-1} = \frac{\pi}{p}\begin{bmatrix} 1 & 1 \\ -1 & 1 \end{bmatrix} \tag{12}$$

The benefit of an isotropic Jacobian goes beyond the numerics, as isotropy means small errors in the drive variables lead to correspondingly small errors in their actuator counterparts, and the other way around. Moreover, the two actuators operate in close cooperation for virtually any single task. Finally, in light of the constancy of the Jacobian, the kinematic relation between rates follows:

$$\dot{\mathbf{w}} = \mathbf{J}\dot{\boldsymbol{\psi}} \tag{13}$$

B. Dynamics

The Euler-Lagrange formulation is applied to derive the equations of motion of the C-drive. The mechanical system has two degrees of freedom, its two independent generalized coordinates being the angular displacements of the motors. The total kinetic energy T of the mechanical system is thus

$$T = \frac{1}{2}\dot{\boldsymbol{\psi}}^T \mathbf{M} \dot{\boldsymbol{\psi}} \tag{14}$$

where $\mathbf{M}$ is the 2×2 generalized inertia matrix, namely,

$$\mathbf{M} \equiv \mathbf{M}_c + \mathbf{M}_h \tag{15}$$

with $\mathbf{M}_c$ and $\mathbf{M}_h$ denoting the generalized inertia matrices of the collar and the rotational parts of the C-drive, respectively, which are given as

$$\mathbf{M}_c = \mathbf{J}^T \begin{bmatrix} m & 0 \\ 0 & (2\pi/p)^2 I_c \end{bmatrix} \mathbf{J}, \quad \mathbf{M}_h = I_h \mathbf{1} \tag{16}$$

in which m and I_c represent the mass and the moment of inertia of the collar around the axis of rotation, respectively; I_h, in turn, represents the moment of inertia of the motor rotor, the coupling, and the screw. The generalized inertia matrix $\mathbf{M}$ of the system thus becomes

$$\mathbf{M} = \begin{bmatrix} I_h + \frac{I_c}{4} + \frac{p^2 m}{16\pi^2} & \frac{I_c}{4} - \frac{p^2 m}{16\pi^2} \\ \frac{I_c}{4} - \frac{p^2 m}{16\pi^2} & I_h + \frac{I_c}{4} + \frac{p^2 m}{16\pi^2} \end{bmatrix} \tag{17}$$

which is apparently constant. Note here that if we specify the mass and the moment of inertia of the collar obeying the relation[3]

$$I_c = \left(\frac{p}{2\pi}\right)^2 m \tag{18}$$

then $\mathbf{M}$ becomes proportional to the 2×2 identity matrix, with the proportionality factor $I_h + I_c/2$. This matrix then becomes isotropic as well. Under this condition, the dynamics of the system becomes decoupled. If one motor of the C-drive accelerates, no reaction torque acts on the other motor. Moreover, since the C-drive is fixed to the machine frame, the potential energy V of the system is constant, as gravity doesn't intervene. In fact, the collar is not completely axially symmetric, but the offset of its center of mass is negligible. The Euler-Lagrange dynamics equations of the C-drive thus become

$$\mathbf{M}\ddot{\boldsymbol{\psi}} = \boldsymbol{\phi} \tag{19}$$

where $\boldsymbol{\phi}$ is the two-dimensional vector of generalized force, which is given by

$$\boldsymbol{\phi} = \boldsymbol{\tau} - \frac{\partial \Delta}{\partial \dot{\boldsymbol{\psi}}}, \quad \boldsymbol{\tau} \equiv \begin{bmatrix} \tau_L \\ \tau_R \end{bmatrix} \tag{20}$$

τ_L and τ_R being the motor torques, while Δ is the dissipation function, namely

$$\Delta \equiv \Delta_v + \Delta_c \tag{21}$$

[3]This relation being difficult to meet, the balance of the paper does not assume an isotropic $\mathbf{M}$.

with Δ_v and Δ_c denoting the Rayleigh dissipation function arising from viscous and Coulomb forces, respectively, which are given by

$$\Delta_v = \frac{1}{2}\beta(\dot{\psi_L}^2 + \dot{\psi_R}^2) + \frac{1}{2}\gamma[(\dot{\psi_L} - \dot{\theta})^2 + (\dot{\psi_R} - \dot{\theta})^2] \tag{22}$$

$$\Delta_c = \delta(|\dot{\psi_L}| + |\dot{\psi_R}|) + \eta(|\dot{\psi_L} - \dot{\theta}| + |\dot{\psi_R} - \dot{\theta}|) \tag{23}$$

In eq. (22), the positive constants β and γ represent the viscous coefficients of the motor rotor with its stator, added to those of the ballscrew support unit bearings, and of the collar with the ballscrews, respectively. In eq. (23), the positive constants δ and η represent, correspondingly, the Coulomb-friction coefficient counterparts of the foregoing viscous coefficients.

Upon differentiation of the second row of eq. (7) with respect to time, one obtains

$$\dot{\theta} = \frac{1}{2}(\dot{\psi_L} + \dot{\psi_R}) \tag{24}$$

Hence, the above angular-velocity differences become

$$\dot{\psi_L} - \dot{\theta} = \frac{1}{2}(\dot{\psi_L} - \dot{\psi_R}), \ \dot{\psi_R} - \dot{\theta} = \frac{1}{2}(\dot{\psi_R} - \dot{\psi_L}) \tag{25}$$

Now, the generalized dissipative-force vector $\boldsymbol{\phi}_d$ is defined as the sum of the contributions of the viscous and Coulomb-friction terms, i.e.,

$$\boldsymbol{\phi}_d = \boldsymbol{\phi}_v + \boldsymbol{\phi}_c, \ \boldsymbol{\phi}_v \equiv \frac{\partial \Delta_v}{\partial \dot{\boldsymbol{\psi}}}, \ \boldsymbol{\phi}_c \equiv \frac{\partial \Delta_c}{\partial \dot{\boldsymbol{\psi}}} \tag{26}$$

Hence,

$$\boldsymbol{\phi}_v = \mathbf{C}\dot{\boldsymbol{\psi}}, \ \mathbf{C} \equiv \begin{bmatrix} \beta + \frac{1}{2}\gamma & -\frac{1}{2}\gamma \\ \frac{1}{2}\gamma & \beta + \frac{1}{2}\gamma \end{bmatrix} \tag{27a}$$

$$\boldsymbol{\phi}_c = \begin{bmatrix} \delta \mathrm{sgn}(\dot{\psi_L}) + \eta \mathrm{sgn}(\dot{\psi_L} - \dot{\psi_R}) \\ \delta \mathrm{sgn}(\dot{\psi_R}) + \eta \mathrm{sgn}(\dot{\psi_R} - \dot{\psi_L}) \end{bmatrix} \tag{27b}$$

with $\mathrm{sgn}(\cdot)$ denoting the signum function[4].

The mathematical model describing the dynamics of the C-drive is thus

$$\mathbf{M}\ddot{\boldsymbol{\psi}} + \mathbf{C}\dot{\boldsymbol{\psi}} + \boldsymbol{\phi}_c = \boldsymbol{\tau} \tag{28}$$

Figure 3 illustrates the block diagram of the C-drive dynamics.

IV. PROTOTYPE

A. Mechanism

The detailed design of the C-drive was guided by a number of criteria, namely: high accuracy; high stiffness; low complexity; modularity; ease of modification; and safety. As this is a proof-of-concept protoype, the design embodiment is not optimized. The fundamental dimensions of the drive were chosen such that the ISMG can perform the standard industry

[4]Simulink^{TM}'s signum function outputs 0 for a vanishing argument.

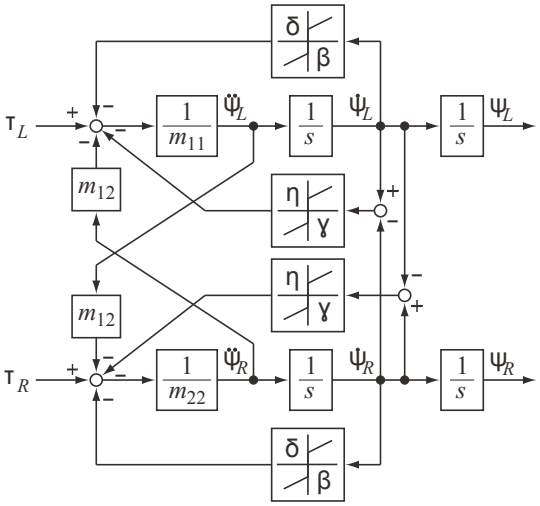

Fig. 3. Block diagram of the C-drive

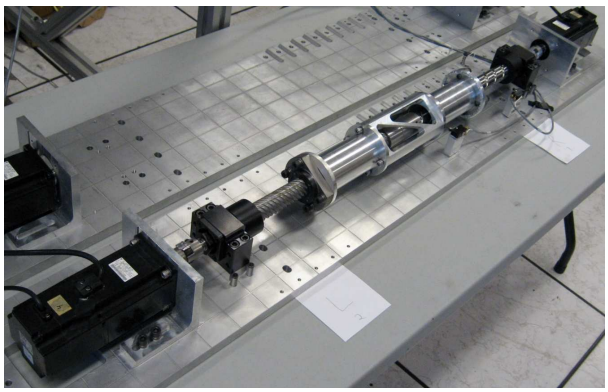

Fig. 4. Photograph of the C-drive and second unassembled base plate

test cycle. The C-drive consists of a precision-ground cast aluminum base plate onto which the motors and ballscrew supporting units are mounted and can be planarly adjusted. A view of the mechanism is shown in Fig. 4. The customized right- and left-handed ballscrews were supplied by THK^{TM}, models WTF3060 and WGF3060, respectively. Their lead is $p = 60$ mm. The supporting units, model BK20, incorporate pairs of angular contact ball bearings that support both radial and thrust loads. In the center of the C-drive, the interface between the two ballscrews is provided by a rotary coupling containing a needle-roller bearing, supporting radial loads.

The collar connects the ball nut of each ballscrew together. It is assembled from three pieces of aluminum 6061 to avoid inaccuracies in coaxiality that arise from turning long components on a lathe, as well as for ease of modification. The middle segment will accommodate an arm of axis normal to the that of the ballscrew, which will be a proximal link of the ISMG, as illustrated schematically in Fig. 1(a). A close-up photograph of the collar and a disassembled ballscrew coupling is displayed in Fig. 5.

The total length of the C-drive is 1.5 m. The stroke of the collar is approximately 210 mm, and terminated at either end by a rubber bumper and a limit switch for safety. In future

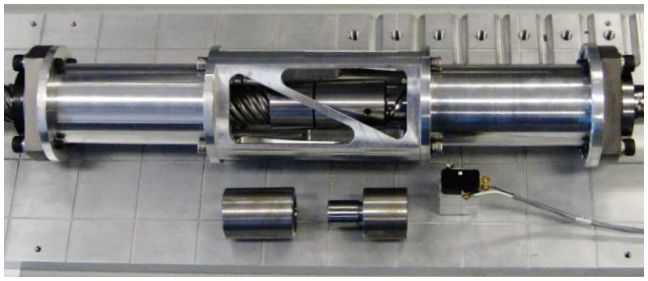

Fig. 5. Close-up photograph of the C-drive, disassembled ballscrew coupling and limit switch

testing, the stroke length will be expanded by shortening the bumpers. This will enable the ISMG to perform the required 300 mm translation during the test cycle.

B. Control System

The C-drive is actuated by two 750 W Yaskawa SGMAH 08AAF4C AC servomotors, rated at 2.39 Nm and 3000 RPM. They are equipped with braking systems and 13-bit incremental shaft encoders [11]. The motors are supplied with two Yaskawa SGDH 08AE-S servomotor amplifiers. The control and feedback signals are acquired by the 24-bit 2 MHz counters of a Sensoray^{TM} 626 PCI multifunction I/O board, housed in the "slave computer" running the real-time operating system QNX^{TM}. The "master computer", running a Microsoft^{TM} Windows operating system, relies on the C-drive user interface in Mathworks^{TM} Simulink^{TM}, using RT-LAB^{TM} from OPAL-RT^{TM}. Programming is done in Simulink^{TM} and compiled as C code on the master computer. This is then loaded onto the slave computer, which runs at a fixed time step of 1 ms.

C. Control Topology

The C-drive is controlled via a PI controller with position feedback and friction compensation. The servomotor amplifiers receive current setpoints and their onboard encoders return a discrete position signal. The PI gains K_P and K_I were determined experimentally. An exhaustive search was performed for K_P by testing at increments between 0.01 and 10 Nm/rad until the system became unstable. K_I was increased until the position offset converged. The gains are

$$K_P = 7.17 \frac{\text{Nm}}{\text{rad}}, \quad K_I = 0.0239 \frac{\text{Nm}}{\text{rad}} \cdot \text{s} \tag{29}$$

D. Modeling and Estimation of the Dissipation Parameters

The Coulomb and viscous friction coefficients β, γ, δ and η, generically refered to as the *dissipation parameters*, were identified experimentally. The friction in the needle-roller bearing coupling the two ballscrews was considered negligible and is thus ignored. The results obtained are reproduced in Table I.

In order to identify the dissipation parameters, smooth, slow motion programs were used, so as to make this identification task independent of the inertial parameters, those appearing in matrix $\mathbf{M}$. Moreover, as the Coulomb-friction model is discontinuous, applying this model verbatim led to

TABLE I

FRICTION COEFFICIENTS

Mechanical Part	Viscous (Nms)	Coulomb (Nm)
Rotational Parts	β = 0.002655	δ = 0.1086
Collar	γ = 0.004333	η = 0.1501

control instability in preliminary tests. The probable causes are given below:

- When $\dot{\psi}_R$, $\dot{\psi}_L$ or $|\dot{\psi}_R - \dot{\psi}_L|$ approach zero, the model introduces noise into the motor control signal because of the noise in the encoder velocity signal, which causes these values to fluctuate around 0.
- Since the signum function has an infinite slope, every direction reversal produces a step impulse in the control signal.

The first point is addressed by incorporating a dead zone (DZ) in the velocity and velocity difference calculations. In a band centered about zero, this function vanishes. The second point is addressed by imposing a rate limiter (RL) to the output of every Coulomb friction term. The coefficients of these two functions were determined experimentally. The resulting friction compensation model is given below:

$$\tau_L = \beta\dot{\psi}_L + \delta RL\left\{\text{sgn}[DZ(\dot{\psi}_L)]\right\} + \frac{1}{2}\gamma(\dot{\psi}_L - \dot{\psi}_R) + \eta RL\left\{\text{sgn}[DZ(\dot{\psi}_L - \dot{\psi}_R)]\right\} \quad (30)$$

$$\tau_R = \beta\dot{\psi}_R + \delta RL\left\{\text{sgn}[DZ(\dot{\psi}_R)]\right\} + \frac{1}{2}\gamma(\dot{\psi}_R - \dot{\psi}_L) + \eta RL\left\{\text{sgn}[DZ(\dot{\psi}_R - \dot{\psi}_L)]\right\} \quad (31)$$

E. Position Control

Three test motions of the collar were implemented: pure translation; pure rotation; and helical motion. A smooth polynomial is used to define the three motion programs. In order to obtain zero velocity, acceleration and jerk at the endpoints, a 4-5-6-7 polynomial $s(\tau)$ [12] is introduced:

$$s(\tau) = -20\tau^7 + 70\tau^6 - 84\tau^5 + 35\tau^4,\ 0 \le \tau \le 1 \quad (32)$$

where τ is nondimensional time and $0 \le s \le 1$.

Based on eq. (13) and the numerical values recorded in Table II, the ranges of motor velocities for the three motion programs are obtained. In the reported tests, the periodic motion programs were implemented at a frequency of 0.5 Hz, a conservative approach for preliminary tests. The first half of the cycle is defined over one second in the form

$$\psi_I(t) = \alpha_I s(t), \quad I = R, L, \quad 0 \le t < 1 \quad (33)$$

where α_I is the motion amplitude, for $I = L, R$, whose values were set as listed in Table II.

F. Test Results

Using the Jacobian **J** appearing in eq. (10), the motor encoder position signal is fed back into the coordinates **w** of the collar. Figures 6–8 display the error measured. Plots of the desired and the achieved displacements are not included, as the corresponding differences are imperceptible. An illustration of these motions is provided in the three videos accompanying the paper.

TABLE II

JOINT-RATE RELATIONS FOR EACH MOTION

Joint Rates	Motion	$\alpha_{\mathbf{I}}$ (rad)
$\dot{\psi}_L = -\dot{\psi}_R$	pure translation	$\alpha_L = 20, \quad \alpha_R = -20$
$\dot{\psi}_L = \dot{\psi}_R$	pure rotation	$\alpha_L = \alpha_R = 20$
$\lvert\dot{\psi}_L\rvert \neq \lvert\dot{\psi}_R\rvert$	helical motion pitch = 180 mm	$\alpha_L = 14, \quad \alpha_R = -28$

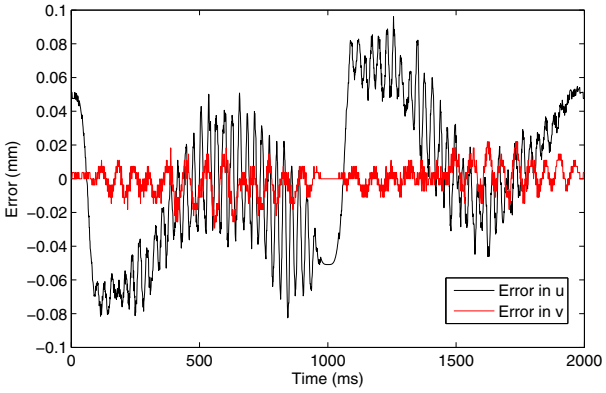

Fig. 6. Error over one cycle in pure translation

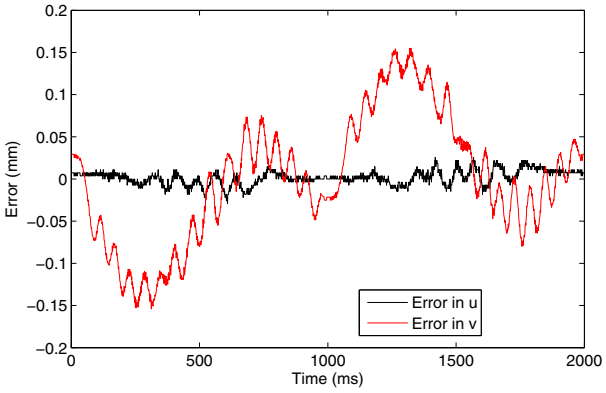

Fig. 7. Error over one cycle in pure rotation

As expected, the error is largest during the accelerating and decelerating portions of the motions, where highly accurate positioning is not needed in PPO. In all tests, the error at the endpoints was below 0.1 mm. From eq. (8), the error in angle θ was never above 0.01 rad at the endpoints.

V. CONCLUSIONS

The overall design process leading to an innovative two-dof robotic drive was outlined in the paper, from the conceptual to the detailed design, followed by prototyping and

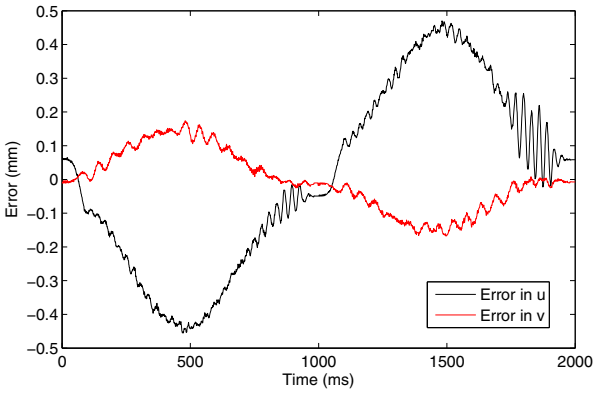

Fig. 8. Error over one cycle in helical motion

preliminary tests. Further work is needed to be able to implement fast motions, as required by PPO. However, the frequency at which the tests were conducted, 0.5 Hz, are not much lower than the fundamental frequency at which the fastest pick-and-place robot operates, namely, 3 Hz. It is expected that, with suitable identification of the drive inertial parameters, motions faster than 3 Hz will be achievable through the use of dynamics compensation. Finally, the integration of the drive and its companion into a parallel SMG, in the coming months, should lead to a prototype capable of competing with those out in the market.

ACKNOWLEDGMENTS

The first author would like to acknowledge the financial support received from MEXT-supported program for the Strategic Research Foundation to Private Universities, 2012–2014, and JSPS KAKENHI Grant-in-Aid for Scientific Research (C) Grant Number 24560314. The third author would like to acknowledge the financial support received from NSERC (Canada's Natural Sciences and Engineering Research Council) through a Discovery Grant and from McGill University via a James McGill Professorship. The support provided by THK CO., LTD. is dutifully acknowledged.

REFERENCES

[1] O. Bottema and B. Roth, 1979, Theoretical Kinematics, Amsterdam: North-Holland Publishing, Co. (also available as a 1990 Dover Publications book).

[2] H. Makino, A. Kato, and Y. Yamazaki, 2007, 'Research and commercialization of SCARA Robot–The case of industry-university joint research and development, *International Journal of Automation Technology*, Vo.. 1, pp. 61–67.

[3] J.-F. Gauthier, J. Angeles, and S. Nokleby, 2008, Optimization of a Test Trajectory for SCARA Systems, in J. Lenarčič and P. Wenger (editors), *Advances in Robot Kinematics: Analysis and Design*, Dordrecht: Springer, pp. 225–234.

[4] O. Company, F. Pierrot, T. Shibukawa, and K. Morita (2001). Four-degree-of-freedom parallel robot. European Patent EP1084802, March 21.

[5] R. Clavel, 1990, Device for the Movement and Positioning of an Element in Space, Patent No. US 4976582, December 11.

[6] C.C. Lee and P.C. Lee, 2010, Isoconstraned mechanisms for fast pick-and place manipulation, in Y. Lou, and Z. Li (editors), Geometric Methods in Robotics and Mechanism Research, Saarbrücken (Germany): Lambert Academic Publishing, pp. 85–99.

[7] W.A. Khan and J. Angeles, 2011, A novel paradigm for the qualitative synthesis of simple kinematic chains based on complexity measures, ASME Journal of Mechanisms and Robotics, Vol. 3, No. 3, pp. 031010-1-031010-11.

[8] J.M. Hervé, 1999, The Lie group of rigid body displacements, A fundamental tool for mechanical design, Mechanism and Machine Theory, Vol. 34, pp. 719–730.

[9] T. Harada, J. Angeles, 2013, Kinematics and Singularity Analysis of a CRRHHRRC Parallel Schönflies Motion Generator, *Proc. CCToMM Symposium on Mechanisms, Machines, and Mechatronics*, May 30-31, Montreal, Paper 12, 10 pp.

[10] G.H. Golub and C.F. Van Loan, 1989, Matrix Computations, Baltimore: The Johns Hopkins University Press.

[11] Yaskawa, Sigma-II Series SGMH/SGDM User's Manual: Servo Selection and Data Sheets, Manual NO SIE-S800-31 1D.

[12] J. Angeles, 2014, Fundamentals of Robotic Mechanical Systems. Theory, Methods, Algorithms, Fourth Edition, New York: Springer.